ELECTRON COLLECTION BY INTERNATIONAL SPACE STATION SOLAR ARRAYS

M.J. Mandell
Science Applications International Corporation
10260 Campus Point Drive, San Diego, CA 92121
Phone: 858-826-1622
E-mail: myron.j.mandell@saic.com

V.A. Davis
B. Gardner
G. Jongeward
Science Applications International Corporation

Abstract

A solar array electron collection model was developed in 1991 for Space Station Freedom, for the purpose of determining the maximum current emission required for the hollow cathode plasma contactor to "ground" the station. Now that the International Space Station (ISS) is on-orbit and the first pair of solar array wings has been deployed, it has been observed that the electron collection by the solar array cell edges is significantly less than that predicted from preflight test results and the original model. A new model was developed that eliminates snapover and takes proper account of the role of plasma density. The model is validated by integration into Environment WorkBench (EWB), which models the station geometry, current-voltage relationships of station elements, point on orbit, plasma environment, v×B induced potentials, and attitude and movement of station solar arrays and performs a circuit analysis to compute the floating potential of the station chassis. These results are then compared with string currents (inferred from measurements of plasma contactor emission currents during targeted DTOs) and from measurements of charging by the Floating Potential Probe (FPP).

History

More than 10 years ago, plasma physicists (the *Space Station Plasma Interactions and Effects Working Group*) pointed out that the floating potential of (then) Space Station Freedom (SSF) would be negative to a major fraction of its solar array voltage. Other spacecraft were known to routinely float around thirty volts negative with no problems, but it was determined that sputtering of thermal coatings was likely at the higher SSF voltages. Therefore, a decision was made to put a hollow cathode plasma contactor on the SSF. To determine the required current capability of the plasma contactor, laboratory measurements of array collection were performed, and a computational model was built. The computational model was based on studies of electrostatic potentials in and near the solar cells performed with the 2-D *Gilbert* code by (then) S-Cubed, Maxwell Laboratories physicists. The model was integrated into the Environment Workbench (EWB). Given the purpose of this effort, the modeling focused on conditions and assumptions leading to the highest plausible solar array collection.

In December of 2001, the first two wings of International Space Station (ISS) solar arrays were deployed and became operational. Measurements indicated that the arrays collected far less electron current from the ionosphere than had been predicted. Thus far, charging has been limited to a few tens of volts, and, in the course of normal operations, occurs only on eclipse exit. However, the specification that no point on the station be more than forty volts negative of the plasma potential is now based on a criticality one hazard due to concern over astronaut safety. Clearly, a new array collection model is required to predict ISS floating potentials to within the accuracy necessary to meet this requirement. There is a need to re-examine the collection model and develop a new or revised model based on first-principles physics that is in agreement with the on-orbit performance of the array.

Previous Collection Model

The solar array collection model developed in 1991 was focused on the sizing of the plasma contactor unit (PCU), specifically to set its maximum current emission capability. As a result, the model parameters were tuned to predict maximum currents. In retrospect, it is not surprising that currents were over-predicted. The two main factors contributing to over-prediction of currents were (1) allowing snapover of any surface for which this was a stable state, and (2) performing calculations (using the *Gilbert* code) only at plasma densities of 1×10^{12} m^{-3}, scaling linearly to other densities. Since present results show that current rises faster than linearly with density, this resulted in overestimated currents at the more common lower densities.

A major uncertainty in the previous treatment was the effective "width" for electrons passing over a potential barrier. Lacking a clear theoretical treatment, this "width" was obtained by measurements of the electrostatic potential plots, even though the plots showed that the potential structure was not amenable to such treatment. In hindsight, the "width" was overestimated.

Nonetheless, the treatment predicted currents in excellent agreement with the laboratory measurements deemed most trustworthy.[1] Also, the model predicted many qualitative features (*e.g.,* temperature dependence) observed in flight, and could be coaxed into quantitative agreement with flight results by simply scaling back the collected current.

The "new" model described here is derived from the "old" model by reviewing the various assumptions and treatments that went into its development, and revising them to give realistic currents over a wide range of orbital configurations and plasma conditions (rather than maximum currents). In doing so, we have the benefit of a substantial set of on-orbit measurements, and need not rely on laboratory experiments under non-space-like conditions, or flight experiments on small coupons.

Components of the Model

Several components contribute to a model of electron current collection from the ionosphere by the ISS solar array cells. Note, however, that the collection model by itself is not sufficient to determine the floating potential of ISS. ISS build geometry and attitude, magnetic field induced voltages, orbital configuration, the amount, distribution and nature of ion-collecting surfaces and other current emitting elements (such as plasma contactors), and possible dynamic effects are additional components of a predictive floating potential model. These components are included in the floating potential module of the Environment WorkBench (EWB) ISS plasma effects tool that is used to validate the array electron collection model.

The components of the array current collection model that need to be treated in some detail are discussed in this section.

Array geometry

The cross-sectional structure of the gap region between solar cells needs to be modeled at a resolution of tens to hundreds of microns. Because this gap cross-section is very small compared with the length of the gap (*i.e.,* the 8 cm side dimension of the solar cells) we can treat array collection as a locally two-dimensional problem.

Surface potentials

The potentials of the coverglass surfaces as well as the insulating surfaces interior to the gap play a role. In this model we consider all these surfaces to be at the potential calculated using the plasma temperature and the angle of the array to the ram (see the Section Surface and Gap Potentials for details). In particular, we do not allow any surfaces to be snapped over. This is one of the major differences between this model of ISS array current collection and the previous one. The decision to suppress snapover is based on the low values of collected current measured in flight.

Gap potential

The "gap" is an imaginary surface between the edges of two adjacent coverglasses and at the same level as the coverglass surface, so that what we refer to as the "gap" actually lies above the true gap surface. This "gap" potential is calculated from the coverglass and cell potentials as described below. Along with the coverglass, this surface forms the boundary of the external space through which electrons are collected, so that its potential is the main determinant of the plasma electron current collected. All but a negligible fraction of electrons crossing the gap surface are eventually collected by the solar cells.

Barrier formation

Under most conditions an electron's trajectory to the gap surface must cross a region of negative (electron-repelling) potential. The least repelling such potential (which occurs on the symmetry plane of the gap as shown in Figure 2) is designated "the barrier" for that set of parameters. The barrier structure results from the superposition of the repulsive coverglass-induced potential and the attractive gap-induced potential. The importance of the barrier is that it reduces the electron population energetically able to reach the gap and be collected by a factor of $e^{-V_b/T}$, where V_b is the magnitude of the barrier and T is the electron temperature.

Orbit-limited collection (corrected by particle tracking)

Rather than trying to identify a geometric width in the potential structure, we assume orbit-limited collection of electrons by the gap surface. As a first approximation, we assume that only energetic considerations limit an electron's ability to reach the gap, and conservation of the distribution function along a trajectory determines the current density to the gap. We refine this estimate by actually tracking electrons (in the reverse sense) to the gap surface. The particle tracking leads to an additional 10% to 30% current reduction, with the larger reductions occurring for the more compact potential structures (*i.e.,* for the higher densities).

String geometry

The array is laid out in compact strings. This provides the gap area per string and the distribution of cell potentials.

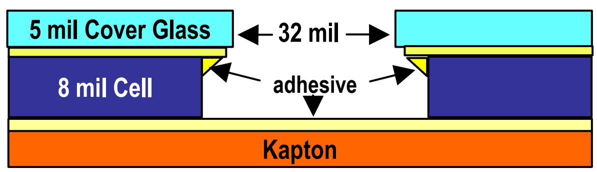

Figure 1. Composition and dimensions of the gap between two solar cells.

Array Geometry

Figure 1 shows the gap region between two solar cells. The cell itself can be at a high potential (up to 160 V), while the other surfaces are at small negative potentials. As mentioned above, we define the "gap" as an imaginary surface extending across the gap at the level of the top of the coverglass, so that the gap surface plus the coverglass surface form a plane boundary to the external space. Note also that the gap dimensions of less than one millimeter are smaller than the Debye length of any anticipated plasma environment encountered by ISS, which would be at least a few millimeters.

An aspect of the gap that has been somewhat controversial is the adhesive coverage on the edge of the solar cell.

Surface and Gap Potentials

We set the potentials of all insulating surfaces to that calculated by current balance between plasma ions and electrons:

$$j_{th} e^{\phi/T} = nev\cos\theta + j_{th}\left(\frac{m_e}{m_i}\right)^{1/2} \qquad (1)$$

where the electron thermal current, j_{th}, is given by

$$j_{th} = ne\left(\frac{eT}{2\pi m}\right)^{1/2} \qquad (2)$$

where T is the electron temperature (eV), v is the spacecraft velocity, θ is the angle between the surface normal and the ram direction, and ϕ is the surface potential. The surface potential varies from about -2T for a ram-facing surface to -5T for a ram-normal surface. We are not concerned with wake-facing surfaces. No snapover is allowed. This estimate is certainly valid over most of the coverglass area. It may well be questioned for the portion of the coverglass near the gap edge and for the gap interior surfaces, as these surfaces are at least somewhat inaccessible to plasma when the cell is on. Nonetheless, we posit departures of surface potentials from these estimates will be small enough to have little effect on the ultimate results.

Potentials in a plasma are screened by the space charge of the ambient plasma, which results from reduced density of the repelled species and acceleration and convergence of the attracted species. For low potentials (linear screening), only the repulsion is important, and the potential falls off exponentially with characteristic distance given by the "Debye length." For high potentials the acceleration and convergence effects are important, so that the geometry of the problem must be self-consistently taken into account. To calculate the gap surface potential we use the finite element electrostatic potential solver of the 2-D *Gilbert* code. *Gilbert* allows us to obtain excellent resolution within the gap while including the full coverglass surface and extending an adequate distance into the external space. In this case, plasma screening has little effect on the gap surface potential both because of the small dimensions of the gap (relative to the plasma Debye length) and because of the high potentials and fields within the gap. As a result, the mean gap potential is a simple linear function of the cell edge potential and the insulator surface (coverglass) potential.

We will see below that we need two different averages for the gap surface potential. For calculating the barrier we use the simple average

$$\langle \phi \rangle_{gap} = 0.01035\phi_{cell} + 0.982\phi_{glass} . \quad (3)$$

For calculating the orbit-limited current collection, however, we use

$$\langle \phi^{1/2} \rangle^2{}_{gap} = 0.00969\phi_{cell} + 0.926\phi_{glass} . (4)$$

Note that these coefficients are appropriate only to the geometry shown in Figure 1.

Barrier Formation

The "barrier potential," ϕ_B, is the least negative potential that an electron trajectory must encounter between its origin in the ambient plasma and the "gap surface." Figure 2 shows the potential structure for "baseline" conditions (n_e=1×10^{11} m^{-3}, T=0.1 eV, ϕ_{cell}=150V). A negative potential barrier of about 0.05 volts is clearly seen about 7 millimeters in front of the gap surface. If a barrier is present, the current to the gap surface is reduced by a factor of exp($-\phi_B$/T). The barrier was calculated using the 2-D electrostatic finite element *Gilbert* code, both in the original 1991 study and in the current work. However, as the barrier potential of order 0.1 volts is a small fraction of the solar cell potential of order 150 volts, it is reasonable to question the accuracy of these calculations. Therefore, an analytic treatment was developed as a check on the numeric results. Also, an analytic treatment is better for use in a full computer model than a suite of numeric results spanning a rather large parameter space.

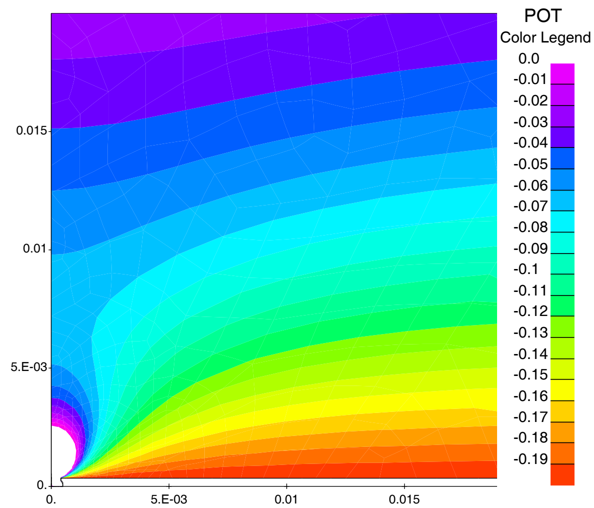

Figure 2. Potential structure above a solar array gap, showing saddle-point potential barrier. Structure is for n_e=1×10^{11} m^{-3}, T=0.1 eV, ϕ_{cell}=150V. White circular area above gap is region of positive potential.

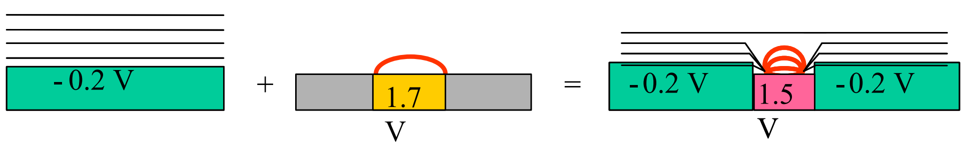

Figure 3. Superposition of coverglass (-0.2 V) potential plus gap surface potential (1.7 V on 0.0 V background) gives spatial potential induced by –0.2 V coverglass with 1.5 V gap surface.

Therefore, we have developed an analytic model for the potential on the symmetry plane (through the center of the "gap surface"). We approximate this potential as a superposition of the potential of a uniform coverglass surface plus the potential of the gap surface, as shown in Figure 3 (Superposition would be exactly correct if the potential were linearly screened. Since the plasma screening is nonlinear, this is an approximation which is good to the extent that the potentials are high enough and the distances short enough that the departure from linear screening is small.)

Coverglass-induced potential

The coverglass-induced potential is the one-dimensional solution to the nonlinear Poisson equation

$$-\varepsilon_0 \nabla^2 \phi = ne(1 - e^{\phi / T}) \qquad (5)$$

where the constant on the right hand side represents the ram ion density (unaffected by low potentials) and the exponential term represents reduced electron density (due to negative potentials comparable in magnitude to the electron temperature). In one dimension, this equation can be integrated once by multiplying by the electric field, $E = -\frac{\partial \phi}{\partial x}$, to get a relation between the electric field and potential.

$$2\varepsilon_0 \frac{d\phi}{dx}\frac{d^2\phi}{dx^2} = -2ne\frac{d\phi}{dx}(1-e^{\phi/t}) \qquad (6)$$

$$E^2 = \frac{2ne}{\varepsilon_0}(Te^{\phi/T} - \phi - T) = \frac{2T^2}{\lambda_D{}^2}\left(e^{\phi/T} - \frac{\phi}{T} - 1\right) \qquad (7)$$

With this relation between the potential and electric field, it is straightforward to integrate the potential outward from the coverglass to obtain the coverglass-induced potential.

The *Gilbert* code was modified to optionally use the above charge density formula in negative potential regions. That brought the *Gilbert* and analytic calculations for the potential above the center of the coverglass into perfect agreement. All *Gilbert* calculations presented here use this charge density formulation.

Gap-surface induced potential

To find the gap-surface induced potential, we solve for the two-dimensional Laplace potential, $\phi(x,y)$, (where x is the distance from the gap center in the plane of the array and y is the distance above the array plane) subject to the boundary condition

$$\phi(x,0) = (\langle\phi_{gap}\rangle - \phi_{glass}) \text{ for } |x| \le w/2 \qquad (8)$$
$$\phi(x,0) = 0 \quad \text{for } |x| > w/2$$

To solve this, we find the Fourier transform of ϕ, g(t):

$$g(t) = \int_{-\infty}^{\infty} dx\phi(x,0)\cos xt = \frac{2\sin(wt/2)}{t}. \qquad (9)$$

Since $\cos xt \exp(-yt)$ satisfies Laplace's equation, we Fourier transform back to find

$$\phi(x,y) = \frac{1}{\pi}\int_0^{\infty} dtg(t)\cos xt\exp(-yt) = \frac{1}{\pi}\int_0^{\infty} dt\frac{2\sin(wt/2)}{t}\cos xt\exp(-yt) \qquad (10)$$

Specializing to x=0 (*i.e.,* on the centerline of the gap) and using the standard tabulated integral

$$\int_0^{\infty} dx\frac{e^{-ax}}{x}\sin mx = \arctan(\frac{m}{a}) \qquad (11)$$

gives $$\phi(0,y) = \frac{2(\langle\phi_{gap}\rangle - \phi_{glass})}{\pi}\arctan\frac{w}{2y} \qquad (12)$$

Of course, this result includes no screening whatsoever. To obtain a maximally screened result, we multiply the Laplacian result by the factor $\exp(-y/\lambda_D)$, where λ_D is the plasma Debye length $(\varepsilon_0 T/ne)^{1/2}$.

Barrier calculation

To determine the barrier potential, we add the coverglass-induced and gap-surface-induced potentials and find the minimum in the resulting curve. We have, however, two curves, depending on whether we consider the gap-surface-induced potential to be screened or unscreened, with the screened version giving a larger barrier. By comparison with *Gilbert* calculations, we set the barrier estimate to 0.76 times the unscreened (smaller) barrier plus 0.24 times the screened (larger) barrier value. Figure 4 shows the two curves for the baseline case of $n_e=1\times10^{11}$ m^{-3}, T=0.1 eV, ϕ_{cell}=150V. The two curves give barrier bounds of 0.0374 and 0.0759 volts, so that our analytic estimate for the actual barrier is 0.047 volts.

Orbit-Limited Collection

Having established that there is (usually) a barrier to electron collection does not determine the electron current actually collected at the gap surface. The well-established way to determine particle collection is to track electron trajectories to the surface in the reverse sense (Figure 5) to see which trajectories correspond to actual environment electrons. Phase space considerations convert this information to the actual current. The approximation that all such trajectories correspond to environment electrons (and thus no particle tracking is necessary) is called the "orbit-limited" approximation.

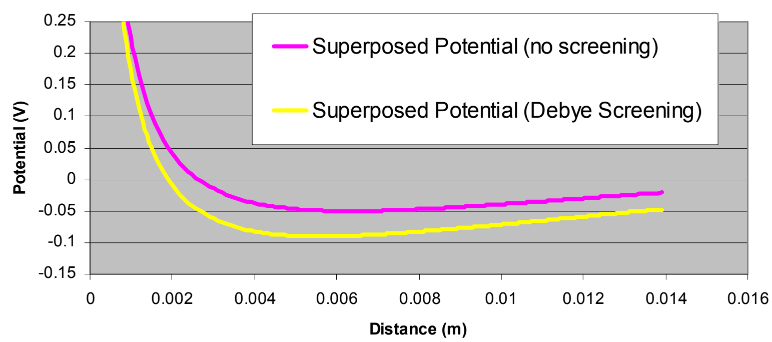

Figure 4. Potential as a function of distance from gap midline, giving screened and unscreened estimates for the barrier potential.

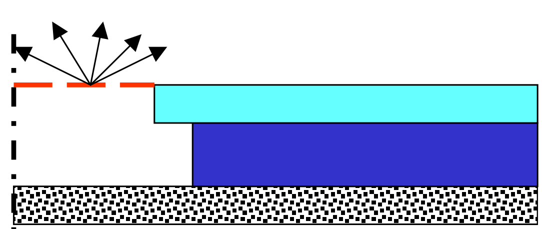

Figure 5. Reverse trajectory scheme to calculate current to surface.

We treat the gap as infinitely long, so that the z-dimension (parallel to the gap length) is ignorable, leaving a two-dimensional problem. The integral to determine the collected current is then

$$j = \frac{n}{2\pi T}\int_{-\pi/2}^{\pi/2} d\theta \int_{\sqrt{2\phi}}^{\infty} (v\cos\theta) v H(v,\theta) dv d\theta e^{-(v^2/2-\phi)/T} \qquad (13)$$

where ϕ is now the potential at the gap surface, and $H(v,\theta)$ is unity for trajectories that connect to the environment and zero otherwise. If, for the moment, we assume H=1 everywhere, we can manipulate the integral to get

$$j = \frac{n}{\pi}\sqrt{2T}\sqrt{\frac{\phi}{T}}\int_0^\infty \sqrt{1+\frac{wT}{\phi}}e^{-w}dw \tag{14}$$

which can be expanded in a series for $\phi >> T$

$$j \cong 2j_{th}\sqrt{\frac{\phi}{\pi T}}\left[1+\tfrac{1}{2}\tfrac{T}{\phi}-\tfrac{1}{4}(\tfrac{T}{\phi})^2+...\right] \tag{15}$$

or integrated exactly $j = 2j_{th}\sqrt{\frac{\phi}{\pi T}}\left\{1+\frac{1}{2}\sqrt{\frac{\pi T}{\phi}}e^{\phi/T}\left[1-erf(\sqrt{\phi/T})\right]\right\}$ (16)

where $j_{th} = ne\sqrt{\frac{eT}{2\pi m}}$ is the normal plasma thermal current.

If we take the potential barrier into account, we get

$$j = \frac{n}{\pi}\sqrt{2T}\sqrt{\frac{\phi}{T}}\int_{\sqrt{\phi_B/T}}^\infty \sqrt{1+\frac{wT}{\phi}}e^{-w}dw \tag{17}$$

$$j = \frac{n}{\pi}\sqrt{2T}\sqrt{\frac{\phi}{T}}e^{-\phi_B/T}\int_0^\infty \sqrt{1+\frac{\phi_B}{\phi}+\frac{wT}{\phi}}e^{-w}dw \tag{18}$$

which eventually leads to

$$j = 2j_{th}\sqrt{\frac{\phi+\phi_B}{\pi T}}e^{-\phi_B/T}\left\{1+\frac{1}{2}\sqrt{\frac{\pi T}{\phi+\phi_B}}e^{(\phi+\phi_B)/T}\left[1-erf(\sqrt{\tfrac{\phi+\phi_B}{T}})\right]\right\} \tag{19}$$

This differs mainly in the exponential reduction by the barrier, since $\phi_B << \phi$ for all gaps collecting substantial current.

Departure from Orbit-Limited Collection

Orbit-limited collection, even with the exponential attenuation by the barrier, provides an upper bound to the collected current. In fact, not all reverse trajectories that are energetically allowed to escape over the gap actually do so; many are attracted back to the originating surface. Such trajectories represent portions of the environment phase space that do not contribute to the surface current. In general, a more compact potential structure leads to a greater fraction of excluded trajectories.

Figure 6 shows the fraction of trajectories connecting to the environment (function $H(v,\theta)$ averaged over angle) for two cases. The fraction goes to zero at the barrier energy, and rises rapidly but continuously to nearly unity. Figure 7 shows the effect on the integrand for the current to the surface.

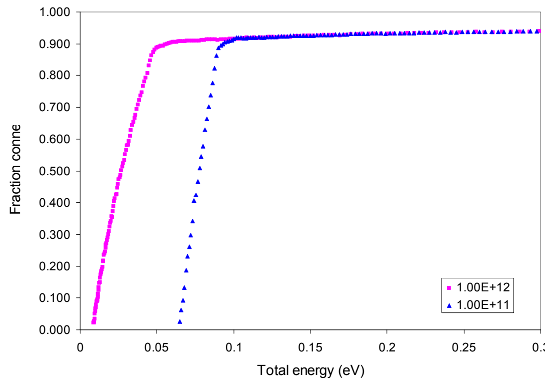

Figure 6. Fraction of trajectories connecting to environment as a function of energy.

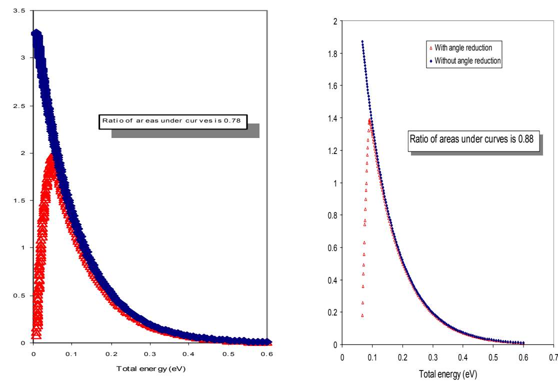

Figure 7. Decrease in integrand due to trajectories that do not connect to environment.

As a result of numerous *Gilbert* calculations, we have developed a simple numeric formula for the reduction in current, <H> due to departure from orbit-limited conditions. The formula is:

$$< H >= 0.89 + 0.62T^2 + 0.039\frac{\phi_{glass}}{T} - 0.02\ln\left(\frac{0.00744}{\lambda_D}\right) \qquad (20)$$

where T is the plasma temperature, ϕ_{glass} is the coverglass potential, and $\lambda_D = \left(\frac{\varepsilon_0 T}{ne}\right)^{1/2}$ is the plasma Debye length. This expression is based on calculations done with temperatures between 0.1 and 0.25 eV (although it is still valid for temperatures down to .05 eV as it changes by only ~2% over this range), plasma densities between 10^{10} and 10^{12} m^{-3}, and coverglass potentials between -0.2 and -0.5 V. It is this expression that defines the parameter range over which the model is valid.

Gap Surface Current Collection

Compiling all of the above results, we find the current per unit length of gap to be

$$\frac{I}{L} = wj_{th}e^{-\phi_B/T} < H >< OL > \qquad (21)$$

where

w = gap width = 8.13×10^{-4} m

j_{th} = plasma thermal current = $ne\sqrt{\frac{eT}{2\pi m}}$

ϕ_B = potential barrier

<H> = current reduction due to departure from orbit-limited current

<OL> = orbit limited current enhancement:

$$2\sqrt{\frac{\phi}{\pi T}}\left\{1+\frac{1}{2}\sqrt{\frac{\pi T}{\phi}}e^{\phi/T}\left[1-erf(\sqrt{\phi/T})\right]\right\} \qquad (22)$$

Note that <OL> is calculated using the square-mean-root gap potential,

$$\left\langle \phi^{1/2} \right\rangle^2_{gap} = 0.00969\phi_{cell} + 0.926\phi_{glass},$$

whereas the potential barrier, ϕ_B, is calculated with the mean gap potential,

$$\left\langle \phi \right\rangle_{gap} = 0.01035\phi_{cell} + 0.982\phi_{glass}.$$

The coverglass potential, ϕ_{glass}, is determined by

$$j_{th} e^{\phi_{glass}/T} = nev\cos\theta + j_{th}\left(\frac{m_e}{m_i}\right)^{1/2}$$

where v is the ram velocity and θ is the angle between the spacecraft velocity and the array normal.

String Current Calculations

To determine the current collected by a string, we need to multiply by the total gap length of the string, and average the collection over the range of cell voltages.

An infinite array of solar cells would have 2 edges per cell. However, the cells are arranged in 4×10 subpanels, leading to 14 extra edges per 40 cells or 2.35 actual edges per cell. With 400 cells per string and 8 cm per edge, each string has a total effective gap length of 75.2 m. Including the gap width gives an effective collection area per string of 0.06 m^2, with is about 2.4% of the actual cell area. Each array or wing contains 82 strings.

Dependence of Solar Array Electron Collection Model on Plasma Environment

Figure 8 below shows how the ISS solar array current, using this model of electron collection by the solar cells, depends on temperature and density. These curves assume sunlit, ram-facing conditions with all 82 strings on and the station chassis held to zero potential (that is, the solar cells on the array have voltages with respect to the plasma of from 0 to 160 volts).

Validation of Solar Array Collection Model

Environment Work Bench (EWB)

We validate the ISS solar array collection model by integrating it into Environment WorkBench (EWB), and comparing calculated array current collection with Plasma Contactor Unit (PCU) emission currents. EWB is an engineering trade study tool for the assessment of space environments effects on spacecraft. EWB was developed under contract to NASA[2] as the ISS plasma interactions and effects analysis tool. As such it has been used to support the plasma contactor design, development and integration efforts and more recently the initial analysis of the ISS Floating Potential Probe (FPP) and Plasma Contactor Unit (PCU) data.

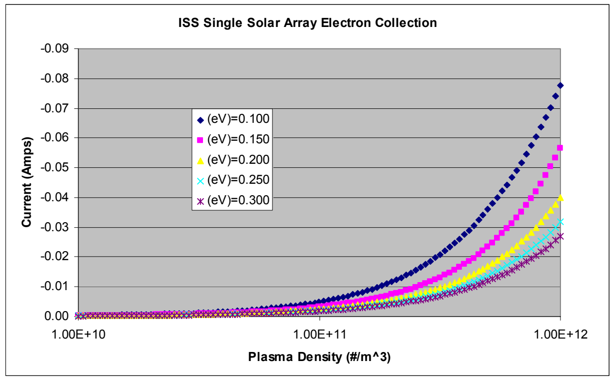

Figure 8. Electron collection of single ISS solar array increases with plasma density and decreases with increasing plasma temperature.

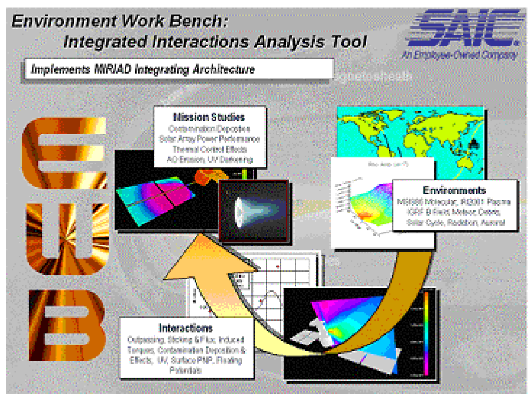

Figure 9. EWB was developed as the ISS plasma analysis tool to support development of the PCUs.

EWB was designed specifically to provide a verifiable methodology for combining the myriad of component interactions that need to be addressed in the calculation of ISS floating potentials. It is more than just a code with many models; it is an integration architecture that supports software in the loop testing.

EWB simulates a fully integrated system. Using ISS two-line element sets, it calculates the position of ISS at the time specified by the user and calculates the plasma, geomagnetic and solar environments at that point on orbit. The ISS model implemented in EWB includes attitude and sun-tracking of the solar arrays. Potentials are calculated over the entire system, including vxB induced potentials, by performing an iterative current balance calculation. Each "component" of ISS, e.g., solar arrays, conducting and insulating surfaces and PCUs has a model of its current/voltage relationship with the surrounding plasma. To change the electron collection of the solar arrays, one need only "plug in" a different model for that one component.

EWB includes standard environment models such as MSIS-86, IRI(90 & 2001), AP-8, AE-8, and IGRF-87, and standard Brouwer and NORAD orbit generators. A database of commonly used spacecraft materials allows selection from a variety of polymers, composites, thermal control coatings, etc., while the constructive geometry system definition enables the user to explore spacecraft configuration issues. Space environment effects models in EWB include electromagnetic and plasma interactions, atomic oxygen erosion, surface contamination (including power system degradation effects), UV absorptivity, meteoroid and debris damage, and others.

Comparison with PCU data

On March 29, 2001 a DTO (delta-to-operations) was performed to shunt and unshunt the ISS solar arrays with the PCUs on. The purpose of this was to observe the jump or dip in the plasma contactor current as a measure of the collection of the arrays. When an array is unshunted, all 82 strings turn on at once, and the current collected on the cell edges is seen in the increased emission from the plasma contactor:

$$I_{pc}(V_s)=I_{mast}(V_s) + I_{body}(V_s)$$
$$I_{pc}(V_u)=I_{mast}(V_u) + I_{body}(V_u) + I_{array}(V_u)$$
$$I_{pc}(V_u)- I_{pc}(V_s)= I_{array}(V_u) + (V_u-V_s)*(dI_{mast}/dV + dI_{body}/dV)$$

V_s is the voltage at the PCU when the arrays are shunted and V_u is the voltage at the PCU when the arrays are unshunted. Since the PCUs are on and grounding the station, V_u is very close to V_s and, to first order the jump in the PC current is just the array current. A series of shuntings and unshuntings of the arrays was performed for each of four orbits as described in Table 1.

Table 1. Times and shunt/unshunt events for each of four orbits on March 29, 2001.

Time	Event
Sunrise + 5:00 (min)	Shunt Port Solar Array (4B)
Sunrise + 5:30	Unshunt Port Solar Array (4B)
Sunrise + 7:30	Shunt Stbd Solar Array (2B)
Sunrise + 8:00	Unshunt Stbd Solar Array (2B)
Sunrise + 10:00	Shunt both Solar Arrays
Sunrise + 10:30	Unshunt both Solar Arrays
Orbit Noon -10:00	Shunt Port Solar Array (4B)
Orbit Noon -9:30	Unshunt Port Solar Array (4B)
Orbit Noon -7:30	Shunt Stbd Solar Array (2B)
Orbit Noon -7:00	Unshunt Stbd Solar Array (2B)
Orbit Noon -5:00	Shunt both Solar Arrays
Orbit Noon -4:30	Unshunt both Solar Arrays

Figure 10 shows a sample of data from the first of four orbits for the March 29 DTO. The magenta line is the PC current. The jumps and dips due to unshunting and shunting of the arrays can be seen clearly. The blue and green points are the number of strings on for 2B and 4B (~26 corresponds to 82 strings on).

Using the newly developed solar array collection model implemented in EWB, we calculate the string current for each of the post sunrise unshunting events for all four orbits. The post-sunrise times were chosen over the pre-noon times because the arrays collect the greatest amount of current when they are in sunlight and into the ram. The data and calculated values are shown in Figure 11, where the red marks are for array 2B and the blue for 4B. The darker square symbols are the data (jump in PCU current normalized to one string) and the lighter round ones, the calculated values. While this is a limited validation effort, these initial results are encouraging.

Calculation of ISS Potentials

The significance of current collection by solar arrays is that it can drive a system negative with respect to the plasma by as much as ~90% of the voltage on the arrays, which in the case of ISS is 160 volts. ISS has a requirement that no point on the station accessible to the astronauts during EVA be more than 40 volts negative of the plasma. Calculation of the station floating potential requires accurate models of the current/voltage characteristics of all surfaces and subsystems. It also requires accurate knowledge of the electron temperature of the plasma. We will discuss these two issues below.

In the case of ISS the major current collecting or emitting components are: electron emission by the PCUs, electron and ion collection by the solar array mast structures, electron and ion collection by the solar array cell edges, and ion collection by exposed conducting surfaces all over the station. In the case of ISS, the one we know the least about that has the largest impact on array driven charging is the effective ion collecting area of the station nodes and truss structures, etc.

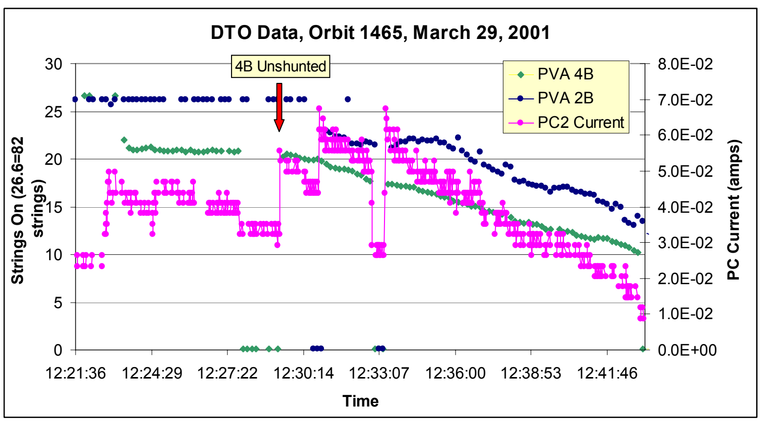

Figure 10. Sample of data from March 29, 2001 DTO. Arrow points to example of 4B unshunting with jump in PCU current.

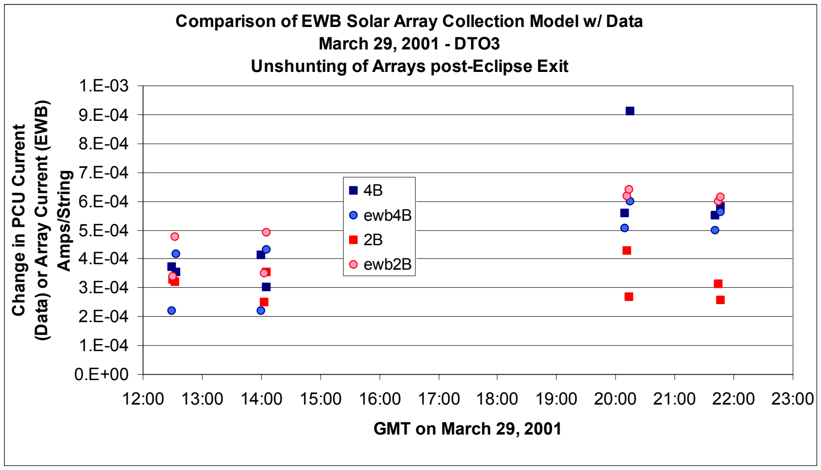

Figure 11. Comparison of string current calculated using EWB, and March 29 DTO data.

Figure 12 shows a typical EWB calculation of chassis potential at the ISS FPP over several orbits on April 11, 2001. These are actually negative potentials but the values have been multiplied by minus one. Also shown is the FPP data for those same orbits. The PCUs were deliberately turned off in order to measure the array driven charging of the station. The ~10 volt lobes are vxB induced potentials while the ~20+volt peaks are ISS charging due to array current collection at eclipse exit. The three EWB calculations shown are done using three different values for the effective ion collecting area of ISS, $25m^2$, $30m^2$ and $35m^2$. This illustrates the effect that ISS ion collecting area has on array driven charging, with a smaller effect on vxB induced potentials. The smaller the ion collecting area, the more negative the system is driven to reduce the electron collection area of the arrays until current balance is achieved.

Another variable that has a large effect on eclipse exit charging levels is the electron temperature of the plasma (as shown in Figure 8), typically .08 to .2 eV for ISS orbit. While the FPP measured the plasma density and temperature, due to the limited range of the Langmuir probe sweep, the environment data is most suspect just when we need it most, *i.e.*, when ISS is charging. Additionally our best models of the plasma environment, such as IRI2001 used here, is climatological. It is not designed to predict the electron temperature at a specific point in time and space at the level of accuracy needed for these calculations.

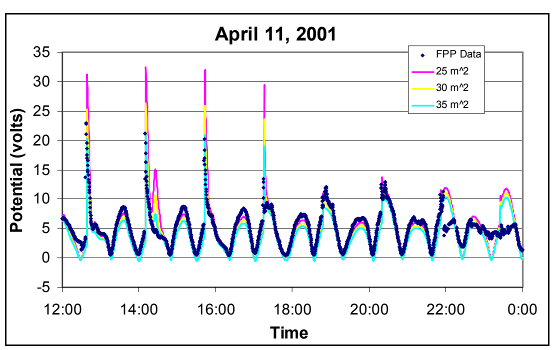

Figure 12. FPP data and EWB calculations of ISS potentials for several orbits on April 11, 2001.

To examine the effect of ion collecting area (A_i) on ISS charging levels over the range of anticipated plasma environments, we use a set of environment data gathered by the AEC satellite[3]. Figure 13 and Figure 14 show calculations done for ~8000 data points. These points were selected to lie within the latitudes seen by ISS, to be sunlit and to be in the morning. The date, time, location, plasma density (n_e) and electron temperature (T_e) were set and the potential at the FPP calculated for each point. Figure 13 shows the maximum potentials calculated for $A_i = 37m^2$ are between 20 and 25 volts (green), while Figure 14, using $A_i=20m^2$, shows maximum potentials of 40-45 volts (red).

All of the FPP charging data was taken over 10 days, from April 10-21, 2001, with a total of about 50 charging peaks. The maximum charging value in the data set is 24 volts which would appear to point strongly to the appropriateness of using approximately $37m^2$ as the effective ISS ion collecting area. However, the small size of our data set and brief time period over which it was taken gives little confidence that we have sampled the entire environment parameter space. We compare the distribution of the data, shown in the Figure 15 histogram, to the distribution of calculated values over the same time period, Figure 16. The calculations were done using $A_i=35m^2$ and IRI2001 calculated environments. The difference in these distributions leads us to believe we are not seeing a wide variation in the plasma environments for these peaks. If we look at the black circles in Figure 13 and Figure 14, we see that the data is consistent with two different areas in environment parameter space depending on what ion collecting area is assumed. In fact, for each value of A_i there is a "region" in n_e-T_e space that fits the range of the April, 2001 FPP data, with T_e being the bigger environmental driver.

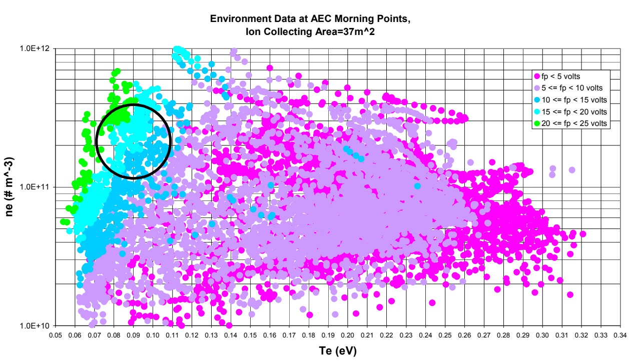

Figure 13. Calculation of ISS potentials at FPP location for ~8000 plasma environment data pairs from the AEC satellite. Assumes 37 m^2 of ion collecting area.

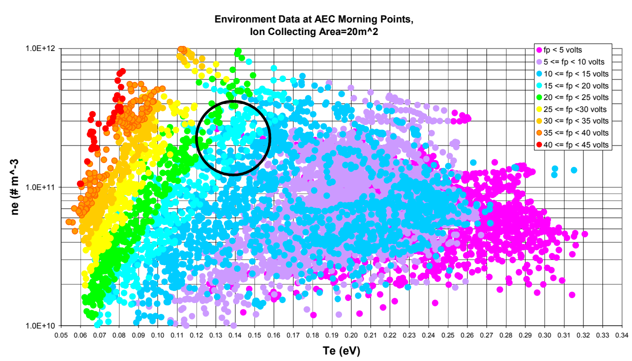

Figure 14. Calculation of ISS potentials at FPP location for ~8000 plasma environment data pairs from the AEC satellite. Assumes 25 m2 of ion collecting area.

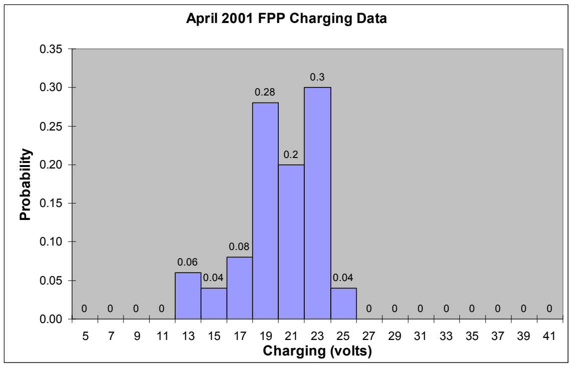

Figure 15. Histogram ISS FPP potentials for 50 observed charging peaks, April 10-21, 2001. Values range from 12 to 24 volts.

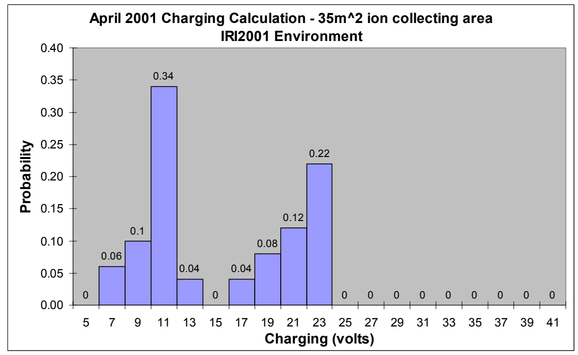

Figure 16. Histogram of calculated ISS FPP potentials for 165 eclipse exits, April 10-21, 2001. Values range from 5 to 23 volts.

Conclusions

Data from the ISS PCUs and FPP are inconsistent with predictions made using the original ISS solar array electron current collection model developed in 1991. With advances in knowledge, codes, and computers, and with on-orbit data for validation, we developed a new model of ISS solar array current collection. The biggest difference between the two models is the addition of a nonlinear electron density dependence and the assumption of no snapover.[4] Preliminary calculations done with the new model integrated into EWB show good agreement with PCU emission current data from the March 29, 2001 DTO. However, maximum ISS potentials cannot be predicted at this time due to our lack of both knowledge of the ISS effective ion collecting area and accurate measurements of the plasma environment. Additionally, we cannot be sure that the next set of solar arrays will collect in the same manner as the present pair. This adds additional uncertainty to the problem.

A Floating Potential Monitor Unit (FPMU) is being developed to fly on ULF1 and should give us the needed environment measurements. What is needed additionally is thorough validation of the array current collection model. This includes revalidation at each PVA-set deployment via targeted DTOs such as that performed on March 29, 2001. This information should allow, at each mission build, calculation of an effective ion collecting area to be used in predictions of 3-sigma worst-case charging of ISS.

References

1. Kaufman, B.A., Chrulski, D., Myers, R.M., “Photovoltaic Plasma Interaction Test II”, Nasa Lewis Research Center, July 14, 1995.

2. EWB 5.0 User’s Reference Manual, NASA/Glenn Contract NAS#-25347, July 31, 1997.

3. Joe Minow, Private Communication.

4. Stevens, N.J., “Review of Biased Solar Array-Plasma Interaction Studies, NASA TM82693, 1981.